Structure and binding kinetics of three different human CD1d-alpha-galactosylceramide-specific T cell receptors

Structure and binding kinetics of three different human CD1d–α-galactosylceramide–specific T cell receptors

Stephan D. Gadola,[1,2] Michael Koch,[3] Jon Marles-Wright,[3] Nikolai M. Lissin,[4] Dawn Shepherd,[2] Gediminas Matulis,[1] Karl Harlos,[3] Peter M. Villiger,[1] David I. Stuart,[3] Bent K. Jakobsen,[4] Vincenzo Cerundolo,[2] and E. Yvonne Jones[3]

[1]Department of Rheumathology and Clinical Immunology, University of Bern, Inselspital, Berne CH-3010, Switzerland
[2]Cancer Research UK Tumor Immunology Group, The Weatherall Institute of Molecular Medicine, Nuffield Department of Medicine, University of Oxford, Oxford OX3 9DS, UK
[3]Cancer Research UK Receptor Structure Research Group, The Henry Wellcome Building for Genomic Medicine, Headington, Oxford OX3 7BN, UK
[4]Avidex, OX14 4RX Abingdon, UK

Invariant human TCR Vα24-Jα18$^+$/Vβ11$^+$ NKT cells (iNKT) are restricted by CD1d–α-glycosylceramides. We analyzed crystal structures and binding characteristics for an iNKT TCR plus two CD1d–α-GalCer–specific Vβ11$^+$ TCRs that use different TCR Vα chains. The results were similar to those previously reported for MHC–peptide-specific TCRs, illustrating the versatility of the TCR platform. Docking TCR and CD1d–α-GalCer structures provided plausible insights into their interaction. The model supports a diagonal orientation of TCR on CD1d and suggests that complementarity determining region (CDR)3α, CDR3β, and CDR1β interact with ligands presented by CD1d, whereas CDR2β binds to the CD1d α1 helix. This docking provides an explanation for the dominant usage of Vβ11 and Vβ8.2 chains by human and mouse iNKT cells, respectively, for recognition of CD1d–α-GalCer.

CORRESPONDENCE
E.Y. Jones:
yvonne@strubi.ox.ac.uk
OR
S.D. Gadola:
stephan.gadola@insel.ch

Abbreviations used: α-GalCer, α-galactosylceramide; CDR, complementarity determining region; CNS, Crystallography and NMR system; DN, double negative; ds, disulfide-linked; iNKT, invariant NKT; J, junctional; PC, phosphatidylcholine; rmsd, root mean square deviation; V, variable.

Invariant TCRαβ-expressing NKT (iNKT) cells comprise highly conserved CD4$^+$ and CD4$^-$/CD8$^-$ (DN) T lymphocyte subsets with important immune regulatory functions (1). In contrast to conventional MHC class I (pMHC) and MHC class II–restricted peptide-specific TCRαβ cells, iNKT cells specifically recognize glycosylceramide ligands presented by non-polymorphic CD1d proteins (2).

α-galactosylceramide (α-GalCer), a glycosylceramide ligand which is not produced by mammals, is widely used as a highly specific antigen for both human and murine iNKT cells. In both species, these cells use precisely rearranged homologous TCR variable (V)α and junctional (J)α segments, namely human Vα24/Jα18 and murine Vα14/Jα18, with minimal or no N-region additions and almost identical CDR3α sequences (3, 4). However, neither a specific Vα nor Vβ chain is required to recognize CD1d protein, since TCRs from autoreactive and nonlipid-specific CD1d-restricted hybridomas use diverse Vα, Jα, and Vβ segments (5, 6). Functional studies using murine iNKT hybridomas have revealed a high degree of iNKT TCR specificity for the carbohydrate portion of the glycolipid ligand (7). Together these facts suggest that the invariant CDR3α loop of iNKT TCRs might be directly involved in recognition of the natural CD1d-bound iNKT antigen.

We have previously described α-GalCer–mediated in vitro expansion of human CD1d–α-GalCer–specific CD4$^+$ and CD8αβ$^+$ T cell populations using diverse TCR Vα, Jα, Vβ, and Jβ chains, demonstrating that TCR Vα segments other than Vα24 can productively rearrange with diverse Jα genes to mediate recognition of CD1d–α-GalCer (8). Interestingly, like iNKT cells, the great majority of Vα24-independent CD1d–α-GalCer–specific cells used polyclonal Vβ11 chains. In addition, in vivo expansion of Vα24-/Vβ11$^+$ CD1d–α-GalCer

V. Cerundolo and E.Y. Jones share senior authorship.
S.D. Gadola, M. Koch, and J. Marles-Wright contributed equally to this work.
The online version of this article contains supplemental material.

tetramer–specific T lymphocytes was recently observed in patients with advanced cancer receiving α-GalCer–pulsed autologous dendritic cells (9). However, in the absence of supraphysiological antigenic in vivo or ex vivo stimulation these Vα24-independent, Vβ11$^+$ CD1d–α-GalCer–specific T lymphocytes are extremely rare (9; unpublished data). Several studies have shown that iNKT cells derive from the same pool of double-positive precursors as conventional T lymphocytes, arguing strongly in favor of their antigen-driven selection (10, 11).

The binding affinities of iNKT TCRs and Vα24-independent Vβ11$^+$ TCRs to CD1d molecules loaded with the natural ligand(s) is not known. However, the observation that Vα24-/Vβ11$^+$ CD1d–α-GalCer–specific T cells can be efficiently expanded both in vitro (8) and in vivo (9) by α-GalCer stimulation suggests that both types of CD1d–α-GalCer–specific TCRs may have similar binding affinities to CD1d–α-GalCer complexes.

To address this hypothesis, we isolated a panel of Vα24$^+$ (iNKT) and Vα24-Vβ11$^+$, CD1d–α-GalCer–specific T cell clones and compared the binding of their recombinant soluble T cell receptors to CD1d–α−GalCer monomers. We extended these studies by determining the atomic structures of the three human TCRs. Based on these results, we suggest a docking model for human TCR binding to the CD1d–α-GalCer complex.

RESULTS

Importance of the CDR3α loop for recognition of CD1d-presented glycolipids

The DN Vα24$^+$/Vβ11$^+$ iNKT clone used for TCR cloning was produced from a previously generated DN iNKT line (8). 13 new Vα24$^-$/Vβ11$^+$ CD1d–α-GalCer–specific T cell clones were generated from a healthy donor, whose Vα24$^-$/CD1d–α-GalCer tetramer$^+$ T cells expanded from background levels to 5.5% within 3 wk in culture after in vitro stimulation with α-GalCer. FACS staining of the clones using CD1d–α-GalCer tetramers showed similar intensities (Fig. S1, available at http://www.jem.org/cgi/content/full/jem.20052369/DC1). However, these clones exhibited different properties regarding their ability to bind to CD1d–α-GalCer monomers and also to express CD4 and CD8 coreceptors (Fig. 1). From these 13 Vα24$^-$/Vβ11$^+$ T cell clones we chose one CD4$^+$ clone, 5E, which exhibited the strongest monomer binding of all CD4$^+$ clones, as well as the CD8αβ$^+$ clone 5B, which showed no detectable monomer binding, for molecular cloning of their TCR α and β chains.

Sequencing data for the cloned variable chains of the three TCRs, iNKT, 5E, and 5B are presented in Fig. 1, A and B. As expected, all three TCRs showed usage of the Vβ11 family, with identical CDR1β and CDR2β, but different CDR3β sequences (Fig. 1 B). The Vβ11 gene segments of iNKT, 5E, and 5B were joined to different Jβ segments, with various N-region deletions and additions. Sequencing of the cloned Vα chain of iNKT confirmed the expected invariant Vα24s1-Jα18 rearrangement and revealed the Vα gene segments used by clones 5E and 5B to be Vα10s1 and Vα3s1, respectively (Fig. 1 A). Alignment of the Vα chain peptide sequences showed 48.9% sequence identity between Vα24 and Vα3.1, 46% identity between Vα24 and Vα10.1, and 44.2% identity between Vα3.1 and Vα10.1 (unpublished data). Surprisingly, Vα gene segments of 5E and 5B were also rearranged to Jα18, resulting in almost identical CDR3α loop peptide sequences for the three TCRs (Fig. 1 A). In all three TCRs two bases had been removed from the 5′ end of the germline Jα18 gene segment, as previously described for other iNKT TCRs (3). No further N-region modifications were seen at the Vα24s1-Jα18 junctional site of our iNKT TCR. In contrast, template-independent N-region modifications could be observed at the Vα-Jα junctions of 5E and 5B. Two N additions were seen at the 3′ end of the germline Vα10s1 sequence in 5E, whereas removal of seven bases from the 3′ end of the germline Vα3s1 sequence as well as insertion of six new nucleotides were found in 5B (Fig. 1 A). Hence, the CDR3α peptide sequences of iNKT, 5E, and 5B differed only with regard to the three amino acids immediately after the conserved disulfide bond-forming Cys90. These results strongly argue for an antigen-driven selection of the Vα24-independent clones, and they suggest an essential role for the CDR3α loop in recognition of the polar head group of CD1d bound glycolipid ligands.

A N-regions of TCRα V-J junctions

Germline Jα18									ccgacagaggctcaaccctgggggaggctata							
Germ Vα24	ATCTGTGTGGTGAGC															
iNKTα	ATCTGTGTGGTGAGC								gacagaggctcaaccctgggggaggctata							
translation	I	C	**V**	**V**	**S**	**D**	**R**	**G**	**S**	**T**	**L**	**G**	**R**	**L**	**Y**	
G. Vα3.1	TTCTGTGCTACGGACG															
5Bα	TTCTGTGCT**c c a ttt**								gacagaggctcaaccctgggggaggctata							
translation	F	C	**A**	**P**	**F**	**D**	**R**	**G**	**S**	**T**	**L**	**G**	**R**	**L**	**Y**	
G. Vα10.1	CTCTGTGCAGGAG															
5Eα	CTCTGTGCAGGAG**c**ggacagaggctcaaccctgggggaggctatac															
translation	L	C	**A**	**G**	**A**	**D**	**R**	**G**	**S**	**T**	**L**	**G**	**R**	**L**	**Y**	

B N-regions of TCRβ V-D-J junctions

Germ Vβ11	TCTGCCAGCAGTGAATA							TRBD						TRBJ2-7*01		
iNKTβ	TCTGCCAGCAGTGAA**aacata***GGGACAG*cctacgagcagtacttcg															
translation	C	A	S	**S**	**E**	**N**	I	**G**	**T**	**A**	**Y**	**E**	**Q**	**Y**	F	
G. Vβ11	TCTGCCAGCAGTGAATA							TRBD						TRBJ1-2*01		
5Bβ	TCTGCCAGCAGTGAAT**cac***GGACAGG***G**attaactatggctacacct															
translation	C	A	S	**S**	**E**	**S**	**R**	**T**	**G**	I	**N**	**Y**	**G**	**Y**	T	
G. Vβ11	TCTGCCAGCAGTGAATA							TRBD						TRBJ1-4*01		
5Eβ	TCTGCCAGCAGTGAAT**tcc***GGGAC***g g** taatgaaaaactgttttttg															
translation	C	A	S	**S**	**E**	**F**	**R**	**D**	**G**	**N**	**E**	**K**	**L**	**F**	F	

Figure 1. Highly similar CDR3α regions in human Vα24-dependent and -independent, Vβ11-positive CD1d–α-GalCer–specific TCRs. Alignments of the Vα-Jα junctions (A) and the Vβ-Dβ-Jβ junctions (B) of dsTCRs iNKT, 5B, and 5E with germline gene sequences are shown (underlined lowercase characters, Jα/Jβ genes; capitals, variable α/β genes; bold lowercase characters, template-independent N-region modifications; italic capitals, Dβ genes; bold capitals, CDR3α/β amino acid sequence).

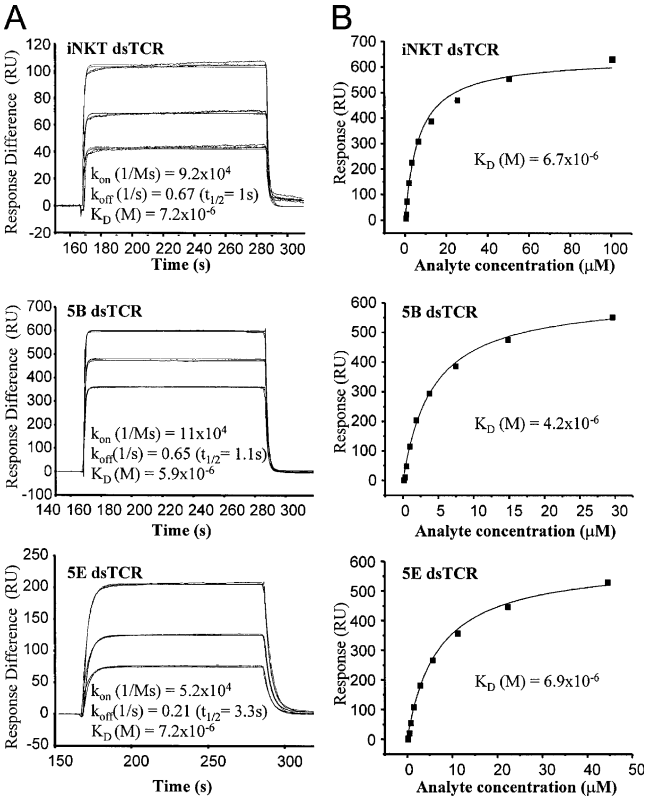

Figure 2. Binding of human invariant NKT and V 24–independent, V 11–positive TCRs to CD1d–α-GalCer. Surface plasmon resonance measurements (BiaCore) for binding of the three dsTCRs iNKT, 5B, and 5E to immobilized CD1d–α-GalCer complex (control proteins: as described in Materials and methods) at equilibrium are shown in A and kinetic measurements are shown in B. ($t_{1/2}$, dissociation half-life; k_{on}/k_{off}, association/dissociation rate constants; K_D, calculated dissociation constant).

Binding kinetics of TCRs iNKT, 5E, and 5B to the CD1d–α-GalCer complex

Soluble versions of the native TCRs iNKT, 5E, and 5B with an engineered disulphide linkage between cysteines introduced at positions 48 and 57 of the TCR Cα and Cβ genes, respectively, (henceforth termed disulfide-linked [ds]TCRs) were generated by in vitro refolding of completely denatured and reduced TCR α and β chain *Escherichia coli* inclusion body proteins. All three dsTCRs refolded with >20% efficiency to produce protein preparations which were >95% pure after ion-exchange and gel-filtration chromatography, as judged by Coomassie-stained SDS-PAGE analysis (unpublished data).

BIAcore surface plasmon resonance analyses of iNKT, 5E, and 5B dsTCRs binding to CD1d–α-GalCer complex are shown in Fig. 2. No binding of these dsTCRs to various control proteins (see Materials and methods) was detected. Conversely, an HLA-A2*01/NY-ESO-1–specific TCR (12) failed to bind to CD1d–α-GalCer complex (unpublished data).

The equilibrium dissociation constants (K_D), based on dsTCR binding to the CD1d–α-GalCer complex at equilibrium in a typical experiment, were 6.7, 6.9, and 4.2 μM for iNKT, 5E, and 5B, respectively (Fig. 2 A). The slightly lower K_D for 5B was observed in three separate experiments. Good agreement was observed between the affinities determined kinetically (the ratio of k_{off} to k_{on}; Fig. 2 B) and those determined by equilibrium measurements (Fig. 2 A). Kinetic binding experiments revealed relatively fast binding kinetics to CD1d–α-GalCer for all three dsTCRs, but the three dsTCRs exhibited significant differences with regard to their k_{off} and k_{on}. In particular, the half-life of dissociation ($t_{1/2}$) was three times slower for dsTCR 5E (3.3 s) compared to iNKT (1.1 s) and 5B (1 s). Since the ability of CD1d–α-GalCer monomers to stain iNKT, 5E, and 5B T cell clones is likely to be determined by the rate of dissociation rather than the affinity (k_{off}), the threefold slower $t_{1/2}$ measured for the interaction of CD1d–α-GalCer monomer with dsTCR 5E compared to 5B could explain the differences in monomer staining described above. These results demonstrate that human TCR Vα chains other than Vα24 can be used by CD1d–α-GalCer–specific TCRs, in combination with Vβ11, to mediate binding to the CD1d–α-GalCer complex that is similar to that of iNKT TCRs. Therefore, the synchronous expansion of iNKT and Vα24$^-$ T cells in response to α-GalCer in vitro (8) and in vivo (9) could be accounted for by a similar binding affinity to CD1d–α-GalCer monomers. To investigate whether Vα24$^-$ and Vα24$^+$ iNKT TCRs differ with regard to their structural frameworks, and to compare their structure to conventional pMHC-specific TCRs, we crystallized the three glycolipid-specific dsTCRs and determined their structures.

Structures of the iNKT, 5E, and 5B dsTCRs

The iNKT dsTCR crystallized in space group C2 with three molecules in the crystallographic asymmetric unit; 5E dsTCR in space group $P3_221$ with a single molecule in the asymmetric unit; and 5B dsTCR in space group $P3_121$, also with a single molecule in the asymmetric unit. The structures of the iNKT, 5E, and 5B dsTCRs were solved by molecular replacement and refined using data to 3.5, 2.25, and 2.6 Å resolution, respectively (Table I). Composite OMIT maps for the α and β chain CDR1 and CDR2 loops in each of the three dsTCR structures are illustrated in Fig. S2 (http://www.jem.org/cgi/content/full/jem.20052369/DC1).

The overall architecture of all three proteins was similar (as shown for the iNKT dsTCR; Fig. 3, A and B) with main chain conformations typical of previously reported TCR structures (Fig. 3, B–D; see following paragraph). Also, as noted for other TCR structures (13) the constant domain of the α chain in the dsTCR structures appeared, with the exception of the CDR loops, to be the most flexible region (as judged from crystallographic B factors). The three copies of the iNKT dsTCR structure were in most respects identical to within experimental error (the second and third copies superimposed onto the first with an root mean square deviation (rmsd) of 0.37 Å and 0.45 Å, respectively for a selected "core set" of Cα atoms; see Materials and methods),

Table I. Statistics for data collection and refinement

Crystallographic statistics			
	5E TCR	**5B TCR**	***i*NKT-TCR**
Data collection			
Resolution range (Å)[a]	30–2.25	18–2.6	30–3.5
(highest resolution shell)	(2.3–2.25)	(2.67–2.6)	(3.62–3.5)
Number of collected reflections	271,030	73,961	75,995
Unique reflections	21,795	13,750	23,622
Completeness (%)	98.8 (89.5)	96.6 (87.4)	98.1 (90.9)
R_{merge} (%)[b]	7.1 (23.8)	12 (55)	18.3 (88.0)
I/σI	31 (7.9)	10.4 (2.2)	6.4 (1.4)
Space group	$P3_221$	$P3_121$	C2
Unit cell dimensions (Å) (a, b, c)	64.5, 64.5, 184.9	64.0, 64.0, 185	289.4, 85.0, 78.9
Unit cell angles (°) (α, β, γ)	90, 90, 120	90, 90, 120	90, 103, 90
Source	ESRF ID14-EH2	SRS Daresbury 14.2	ESRF ID14-EH1
Model refinement			
Resolution range (Å)	30–2.25	18–2.6	30–3.5
Number of reflections (test set)[c]	20,555 (1,098)	13,033 (656)	23,453 (1,193)
R_{cryst} (%)[d]	18.8	21.7	28.3
R_{free} (%)[e]	26.8	31.8	35.0
Number of nonhydrogen protein atoms	3,436	3,392	10,330
Number of water molecules	286	61	0
Average B factors			
Protein (Å^2)	34.4	39.6	46.1
Water (Å^2)	30.2	23.5	n/a
r.m.s. deviation from ideality			
Bond lengths (Å)	0.012	0.009	0.006
Bond angles (°)	1.41	1.32	1.20
r.m.s. deviation B factors (bonded atoms)			
Main chain (Å^2)	2.3	1.8	2.4
Side chain (Å^2)	3.1	1.9	4.6
Ramachandran plot			
Favored (%)	90.4	83.3	78.8
Allowed (%)	8.3	15.4	19.0
Generous (%)	1.0	0.3	1.7
Unfavored (%)	0.3	1.0	0.5

[a]Values in parentheses refer to the highest resolution shell of data.
[b]$R_{merge} = \Sigma h \Sigma i \mid Ii(hkl) - <I(hkl)> I / \Sigma h \Sigma i Ii(hkl)$, where $I_i(hkl)$ is the "ith" measurement of reflection hkl and $<I(hkl)>$ is the weighted mean of all measurements of reflection hkl.
[c]Test set is a randomly chosen set of reflections omitted from the refinement process.
[d]$R_{cryst} = \Sigma h \mid\mid F_{obs}(hkl)| - | F_{calc}(hkl)|| / \Sigma h|F_{obs}(hkl)|$, where F_{obs} and F_{calc} are the observed and calculated structure factor amplitudes, respectively.
[e]R_{free} is equivalent to R_{cryst} but calculated for the test set of reflections.

and unless otherwise stated the first copy was taken as the representative structure in the following analyses (Fig. 3B).

Structural comparison of human CD1d-glycolipid– and CD1d-pMHC–specific TCRs

Superposition of our three dsTCRs with previously determined crystal structures of pMHC-specific TCRs resulted in rmsd values (based on a "core set" of framework residues; see Materials and methods) ranging from 1.1 to 2.0 Å for comparisons with human TCRs and 1.5 to 2.1 Å for mouse TCRs (Fig. 3 B). These rmsd values were somewhat inflated by differences in the relative domain orientations between TCRs. Taken in isolation, the CD1d–α-GalCer–specific Vα domains superimposed with rmsd values of 0.3–1.0 Å with each other and 0.5–2.0 Å with those of pMHC-specific human TCRs, whereas the Vβ regions had a rmsd range of 0.3–0.7 Å compared with each other and 0.8–1.5 Å with other human TCRs. These comparisons revealed no systematic variations in framework structure that distinguished the CD1d–α-GalCer–specific human dsTCRs.

The CDR1 and CDR2 loops of the three CD1d–α-GalCer–specific TCRs were also comparable to those of the pMHC-specific TCRs (Fig. 3, C and D). Al-Lazikani et al. (14) have grouped the CDR1 and CDR2 loops of TCRs into

sets of canonical structures based on loop length and the conservation of certain key residues. Our analysis of the CDR loops of the three CD1d–α-GalCer–specific TCR structures demonstrated that they conform to these canonical structures.

CDR loop architecture

CDR loop architectures for the iNKT, 5E, and 5B dsTCRs are displayed in Fig. 4. The CDR1α loop of the dsTCR iNKT corresponds most closely to the α1-2 canonical structure of Al-Lazikani et al. (14). In contrast, the CDR1α loops of dsTCRs 5E and 5B both have α1-1–type canonical structures; in 5E the Ser26-Oγ forms a hydrogen bond to the backbone nitrogen of Ser28 and packs against the edge of the Phe30 aromatic ring, whereas in 5B the edge of the Tyr26 ring packs against the aliphatic side chains of Ile30 and Leu33 (Fig. 4 A and Fig. S2). The iNKT TCR CDR2α loop has a α2-2 canonical structure as does the CDR2α loop in dsTCR 5B. Conversely, the CDR2α loop of TCR 5E adopts a type II turn conformation, which is characteristic of the α2-4 canonical structure, with a main chain hydrogen bond between the carbonyl oxygen of Thr52 and the nitrogen of Glu54 (Fig. 4 B and Fig. S2). Thus, CD1d–α-GalCer–specific TCRs can show substantial differences in the structures of their CDR1α and CDR2α loops but none deviate from standard TCR architectures.

In contrast to the variation in their α chains, all three CD1d–α-GalCer–specific TCRs used Vβ11 and their CDR1β and CDR2β loops share identical main chain conformations. The CDR1β loop is a β1-1 canonical structure, with Oε1 and Nε2 of Gln26 forming hydrogen bonds with the main chain nitrogen of Met28 and carbonyl oxygen of His30, respectively. The CDR2β loop is a β2-1 canonical structure, with the carbonyl oxygen of Ser50 forming hydrogen bonds to the main chain of nitrogen of Gly52 (Fig. 4, C and D and Fig. S3, available at http://www.jem.org/cgi/content/full/jem.20052369/DC1).

No canonical structures have been described for the much more diverse CDR3 loops. The sequences of the CDR3α loops for TCRs iNKT, 5E, and 5B differ only for residues 91–93 (which neighbor the disulfide bond forming Cys90 of the conserved TCR framework). These sequence differences are therefore located in a part of the CDR3α loop which is unlikely to be directly involved in binding to the CD1d–α-GalCer complex. However, these sequence differences, combined with differences in the environment, which the CDR3α loops experience within the iNKT, 5E, and 5B dsTCR crystals, result in substantially different main chain conformations. Within this range of conformations, the CDR3α loop structures of TCRs 5E and iNKT are more similar to each other, compared to TCR 5B. This may, at least in part, reflect in the sequence of 5B, where residues 92 and 93 are a proline residue and a bulky phenylalanine, respectively, whereas small residues occupy these positions in iNKT and 5E. However, the conformational variations are also in line with the flexibility characteristic of many αβTCR CDR3 loops (for review see references 13, 15).

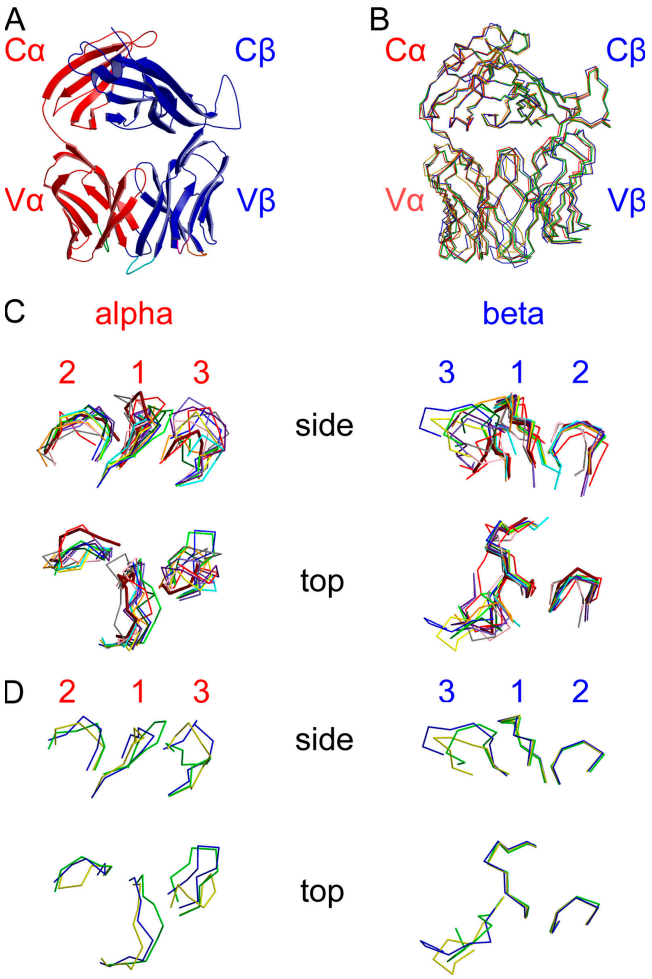

Figure 3. Overall structure of the three TCRs and comparison with the canonical MHC binding TCR structures. (A) Ribbon plot of the iNKT-TCR structure with α-chain shown in red and β-chain in blue. The constant domains are at the top and the variable domains at the bottom of the panel. CDR loops are color coded: CDR1α (green), CDR2α (orange), CDR3α (dark blue), CDR3β (light blue), CDR2β (yellow), and CDR1β (magenta). (B) Superposition of the Cα traces of the dsTCRs: iNKT, first molecule in the asymmetric unit (green), second (red), and third (gray), 5E (yellow), and 5B (blue). Orientation is the same as for A. (C) Close-up view of the hypervariable loop structures from all published canonical MHC class I–binding TCRs and the three CD1d–α−GalCer–specific dsTCR α chains (left two figures) and β chains (right two figures), each seen from the side (top) and top (bottom). 5E dsTCR is shown in yellow, 5B dsTCR in blue, iNKT dsTCR in green, and the other TCR chains are shown in the following colors: 1A07, orange; 1BD2, dark green; 2BNQ, indigo; 1LP9, red; 1MI5, pink; 1OGA, cyan; 1KGC, mid-grey; and 2BNU, slate blue. The mouse MHC class I binding TCR 2CKB, which we used for our docking of the iNKT dsTCR, onto hCD1d is depicted in thick brown lines. (D) The same presentation as in C shown only for the three dsTCR structures: iNKT in green, 5E in yellow, and 5B in blue.

In contrast to the conservation seen for the CDR1β and CDR2β loops, the CDR3β loop sequences and hence structures are different for each of the three CD1d–α-GalCer–specific TCRs. The CDR3β loop of the iNKT dsTCR

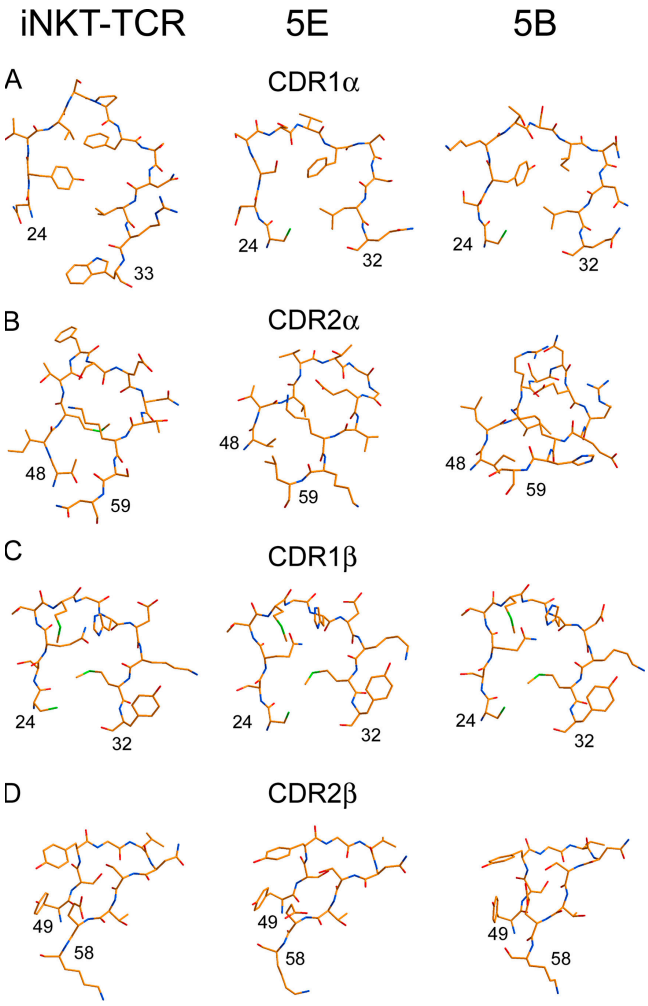

Figure 4. Architectures of CD1d–α–GalCer–specific TCR CDR1 and CDR2 loops. The loop architectures are shown for the CDR1α (A), the CDR2α (B), the CDR1β (C), and the CDR2β loops (D) of the three dsTCR structures iNKT (left), 5E (middle), and 5B (right). Carbon atoms are depicted in yellow.

structure adopts an extended conformation, with main chain hydrogen bonds between the Gly99 nitrogen and the Ala101 carbonyl oxygen as well as between the Glu96 nitrogen and the Tyr102 carbonyl oxygen. The TCR 5E also has an extended CDR3β loop, again with several main-chain hydrogen bonds stabilizing this conformation. In the structure of TCR 5B, the CDR3β loop is less extended with more interactions between side chains than in TCR 5E.

Overall, the CD1d–α-GalCer recognition surfaces (formed by the CDR loops) of dsTCRs 5E and *i*NKT are quite similar, whereas dsTCR 5B has more positively charged residues on its surface (Fig. S5, available at http://www.jem.org/cgi/content/full/jem.20052369/DC1).

A model for CD1d recognition

Our analysis showing that the CDR loops of CD1d–α-GalCer–specific dsTCR structures resemble those of pMHC-specific TCRs supports the idea that the mode of binding of TCRs to CD1d–lipid and CD1d–pMHC complexes is similar. The current data base of TCR-pMHC crystal structures in general shows the TCR CDR1 and 2 loops making contact with the α1 and α2 helices of the antigen binding site and the CDR3 loops making the most intimate contact with the antigen (for review see references 13, 15); however, the orientation, and position, of the TCR relative to the pMHC antigen binding groove can vary significantly between complexes. Thus, we may expect that docking models for TCRs to CD1d–α-GalCer may provide some useful general insights but will not reliably predict the detailed interaction interface. To generate such models, we selected as a template for the relative TCR to antigen binding groove orientation a pMHC-TCR crystal structure which minimized steric clashes between the TCRs and CD1d–α-GalCer (see Materials and methods).

Docking models (Fig. 5, A–C) were generated for the iNKT, 5B, and 5E TCR crystal structures described above and the previously reported crystal structure of human CD1d–α-GalCer (PDB code 1ZT4) (16). In all three models, the CDR1 and CDR2 loops of the TCR Vα and Vβ main chains make sterically acceptable contacts with the CD1d–α-GalCer molecule. The CDR1α loops are predicted to contact the CD1d surface in the region of α1 helix residues 61–69 and the CDR2α loops in the region of α2 helix residues 156–160. The interactions of the CDR2β loop are particularly noteworthy. Arg79 points, finger-like, from the CD1d α1 helix (Fig. S4) into a shallow groove, formed by the CDR2β loop and present in all three TCRs (Fig. 5 D). This conserved surface is formed by a set of polar and charged residues (Tyr49, Tyr51, Ser55, and Glu57), which could mediate electrostatically favorable interactions with Arg79. Arg79 is conserved between mouse and human CD1d (17, 18); however, comparison with the three currently available mouse CD1d structures (19–21) (accession nos. 1CD1, 1Z5L, and 1ZHN) indices that, certainly before TCR binding, this residue is conformationally very flexible (Fig. S4).

Our models suggest that the TCR CDR3α and CDR3β loops plus the CDR1β loop are responsible for making interactions with ligands presented by CD1d. Notably, the positively charged Lys32 side chain in the CDR1β loop appears to be a good candidate for mediating specific recognition of the carbohydrate head group of α-GalCer (Fig. 5 E). Previous studies have suggested that CD1/glycolipid-specific TCRs bind CD1 in a manner similar to that predicted by our docking models such that the CDR3 loops are positioned centrally over the polar head group of the glycolipid ligand (22–25) (Fig. S5). All three dsTCR crystal structures exhibit a large surface cavity between the CDR3 loops of the α and β chains (Fig. S5), which could potentially, with some conformational changes of the CDR3 loops, clamp around the sugar head group of the antigen α-GalCer. Such conformational flexibility would be consistent with the differences in conformation observed between the CDR3α loops in our three unliganded TCR structures. Certainly some conformational

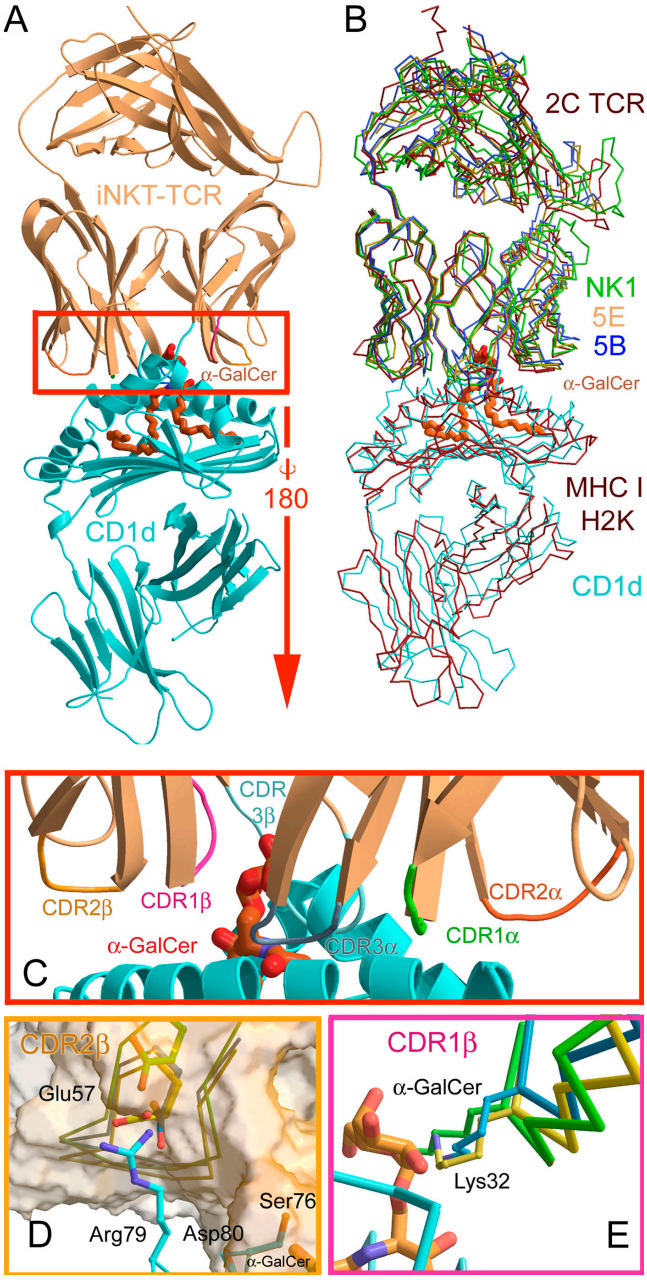

Figure 5. Docking of the TCRs onto CD1d, based on the TCR 2C–pMHC complex. (A) Ribbon plot of the modeled iNKT dsTCR–CD1d complex structure with CD1d shown in cyan and iNKT in gold. For the interface, the α-GalCer molecule is shown in orange and the CDR loops are depicted in the color coding of Fig. 2 A. (B) Structural alignment of the modeled TCR–CD1d complexes (iNKT: first molecule in the asymmetric unit [green], 5E [yellow], and 5B [blue]. The CD1d molecule is shown in cyan, α-GalCer in orange. The Cα-trace for the TCR 2C-pMHC H2K (PDB entry: 2CKB) complex is shown as thick brown lines. (C) Close-up view of the iNKT CD1d interface from A focused on the CDR loops. For better visualization, the orientation is rotated from that in A by 180° around the y axis. (D and E) Close-up views of the model complex centered on the CDR1β (D) and 2β (E) loops of the three dsTCRs, depicted in the same colors as in B. Side chains are shown for residues which the model implicates in TCR–CD1d–α-GalCer binding. For D, the molecular surface of the iNKT-TCR is shown, with Arg79 from CD1d fitting into a surface depression (in the crystal structure of the unliganded CD1d this side chain is flexible and has here been slightly rebuilt).

changes in the CDR3α and CDR3β loops of the three CD1d–α-GalCer–specific TCRs are predicted by the current docking studies since in all three model complexes these loops (in their unliganded conformations) made significant steric clashes with the CD1d–α-GalCer.

DISCUSSION

The highly conserved CD1d-restricted iNKT cells are believed to bridge innate and adaptive immune responses by exerting potent immune regulatory functions (1). A key question of iNKT biology is how their TCRs recognize CD1d-presented glycolipid ligands. Remarkably, human and mouse iNKT use the homologous Vα24/Jα18 and Vα14/Jα18 gene families, respectively, for TCRs that also share almost identical amino acid sequences in their CDR3α loops (3, 4). On the other hand, diverse TCRs from autoreactive and nonlipid-specific CD1d-restricted hybridomas can recognize CD1d proteins (5, 6). It has therefore been proposed that human and mouse iNKT recognize the same or at least a very similar CD1d-bound ligand via their invariant CDR3α loop. In support of this hypothesis, it has been previously shown that discrete differences in the carbohydrate moiety of the CD1d ligand steer recognition by iNKT TCRs (7).

Here we provide further evidence for direct recognition of CD1d-bound ligands by the CDR3α loop. First, the high degree of conservation of CDR3α peptide sequences between iNKT clones and different native CD1d–α-GalCer–specific $Vα24^{-}/Vβ11^{+}$ clones argues strongly for the CDR3α loop having a key role in ligand recognition. Second, N-region modifications used by the two Vα24-independent T cell clones clearly indicate their antigen-driven selection. Conversely, our findings demonstrate that Vα24 gene segments are not essential for CD1d–α-GalCer recognition. Consistent with these observations, BiaCore analysis showed that human invariant $Vα24^{+}$ TCR and $Vα24^{-}$ independent $Vβ11^{+}$ TCRs have similar binding affinities to CD1d–α-GalCer monomers. These results raise the question as to whether the dominant usage of Vα24 TCR chains by iNKT TCRs is actually due to favorable binding to CD1d molecules loaded with the natural ligand(s) or to other factors. Although we cannot rule out the former possibility, it is possible that the observed dominance of Vα24 gene segments over other Vα gene segments in human CD1d–α-GalCer–recognizing T lymphocytes in vivo could be due to early terminal deoxynucleotidyltransferase–independent rearrangement of Vα24-Jα18 segments, as is the case for the invariant TCR gamma and delta chains of murine DECs (26). Consistent with this hypothesis mice lacking terminal deoxynucleotidyltransferase are still capable of generating CD1d–α-GalCer–recognizing T lymphocytes (27).

Although our measurements are within the range of K_Ds measured for human and mouse class I– and class II–restricted TCR (28), previous BiaCore studies with mouse NKT TCR have reported considerably higher binding affinities to mouse CD1d–α-GalCer monomers, with K_D values ranging from 0.098 to 0.35 μM (29–31). Our studies do not highlight any structural characteristics that could explain the difference in affinities between mouse and human iNKT TCR. One of several possible explanations could be the different nature of the recombinant TCRs used in the two studies, i.e., single-chain mouse TCRs (previous studies) versus ds human TCRs (this study).

A direct role for the CDR3α loops in peptide specificity of pMHC-restricted TCRs was originally confirmed in experiments with transgenic mice, where fixation of both a rearranged Vβ chain and the peptide antigen resulted in selection of only one Vα chain (32). Likewise, a fixed Vα chain and peptide antigen resulted in selection of different but restricted Vβ chains (32). Crystal structures of peptide-specific TCRs in complex with their pMHC ligands have revealed that the TCRs bind in a relatively conserved diagonal orientation, thereby positioning their CDR3α and CDR3β loops over the peptide-containing antigen-binding groove (33, 34). The structural similarity of MHC class I and CD1d molecules (16, 19), plus the high degree of structural conservation between our three CD1d-specific TCRs and pMHC-specific TCRs, is suggestive of similar mechanisms for TCR/MHC and TCR/CD1d recognition. We therefore generated a TCR–CD1d docking model based on the available database of crystal structures for TCR/MHC class I complexes. Our analysis of the functional and structural data for CD1d–α-GalCer and cognate TCRs in the context of the TCR–CD1d docking model provides several highly plausible insights into details of the TCR–CD1d interaction. Consistent with previous modeling exercises for TCR–CD1 binding (22–25) the current model predicts that all three CD1d–α-GalCer–specific TCRs position their CDR3α and CDR3β loops in close proximity to the carbohydrate head group of the CD1d-bound α-GalCer. In addition, as seen in TCR-pMHC recognition systems (34) the model also implies that the CDR3 loops must undergo conformational changes between the unliganded and CD1d-liganded states. Such changes are potentially important in allowing TCR recognition of other CD1d-presented antigens (such as isogloboside or phosphatidylinositol mannoside) (35, 36). Given the inaccuracy of the docking model, we cannot comment in detail on these TCR–ligand interactions. However, the model does provide new insights into the potential contribution of the CDR1 and CDR2 loops to CD1d binding.

The peptide sequences of the CDR1α and CDR2α loops are not conserved between our three CD1d-recognizing TCRs although these TCRs exhibit almost identical avidity for CD1d–α-GalCer. Moreover, human Vα24 and mouse Vα14 germline CDR1α and CDR2α sequences are not similar, nor are the CD1d residues conserved between human and mouse at the contact sites predicted by our docking models.

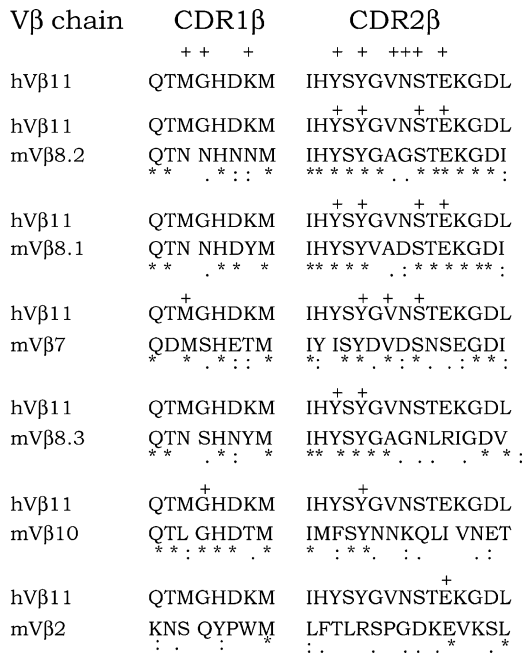

Figure 6. CD1d-contacting residues are conserved within CDR2 loops of dominant human and mouse iNKT TCR V chains. Alignments are shown of the CDR1β and CDR2β regions of the human TCR Vβ11 chain with different TCR β chains of mouse iNKT TCRs are shown. Amino acids predicted by the docking model to directly contact CD1d by the docking model are marked by "+" above the sequence. An asterisk "*" under the sequence symbolizes identical residues; conserved amino acid substitutions are denoted by ":" and semiconserved substitutions by ".". (Alignments were carried out using ClustalW sequence alignment. http://www.ebi.ac.uk/clustalw/).

Thus, the CDR1α and the CDR2α loops may either not be important in stabilization of TCR–CD1d binding, or may make their contribution to binding by several equally viable alternatives (depending on germline CDR1α and CDR2α sequence) which involve no conserved interactions.

In contrast, based on the observation that randomly chosen Vβ8.2 chains can confer strong affinity to mouse Vα14-Jα18 TCR (31), and the fact that CDR3β loops used by iNKT are highly polymorphic (27), it has been suggested that CDR1β and/or CDR2β, rather than CDR3β, may be important for steering iNKT TCR avidity. The model presented here revealed a surprisingly good docking of the CDR2β loop onto the CD1d protein surface. Two of the CD1d residues involved in this putative interface, Arg79 and Asp80, have previously been predicted to be critically involved in TCR binding on the basis of site-directed mutagenesis studies (24, 29). Moreover, alignment of the human Vβ11 gene with the related mouse Vβ8.2 gene revealed 89% identity of their CDR2β sequences, whereas the overall identity of these two Vβ amino acid sequences was only 54% (Fig. 6). Furthermore, all five CD1d residues contacted by CDR2β in our model are conserved between the otherwise only 66% identical human and mouse CD1d protein sequences. Although human iNKT TCRs exclusively use

Vβ11, mouse iNKT can use other Vβ chains in addition to the predominantly used Vβ8.1 and Vβ8.2 chains (37). Recent evidence has indicated that the dominant use of certain Vβ chains by mouse iNKT is directly related to the Vβ chain's contribution to TCR avidity (38, 39). In particular, Vβ8.2 chains have been demonstrated to confer higher TCR avidity to Vα14-Jα18 iNKT compared to the subdominant Vβ7 chains (39). Interestingly, comparison of the complete human Vβ11 CDR2β sequence as well as of the five predicted CD1d-contacting CDR2β residues with the different mouse iNKT-associated Vβ chains showed that mouse Vβ8.2 was most similar to human Vβ11, followed in order by Vβ8.1, Vβ7, and Vβ8.3. Together these facts demonstrate a close link between the CDR2β loop structure and the dominant use of Vβ11 and Vβ8.2/Vβ8.1 chains by human and mouse iNKT, respectively. Similar structural principles have been shown to govern Vβ chain usage by certain immunodominant pMHC-specific TCRs such as human HLA-A2*01– restricted, influenza matrix protein–specific TCRs (40).

Comparison of the human CD1d–α-GalCer crystal structures (16) with the recently solved structure of mouse CD1d loaded with the self-ligand phosphatidylcholine (PC) (21) shows important differences in the positioning of the antigenic headgroup, which are caused by both inherent differences of anomeric headgroup conformation as well as interactions of the headgroup with CD1d protein. In contrast to the galactose of α-GalCer, the phosphate of the PC headgroup makes a charge interaction with Arg79 of the α2-helix. The authors suggest a model for iNKT–TCR interactions with CD1d–antigen complexes based on a comparison of surface clefts which provide suitable docking sites for TCR CDR loops in MHC peptide and CD1d–antigen structures. From this analysis, the PC headgroup was predicted to be contacted by CDR3β and CDR1 (21). These predictions are fully consistent with our docking model for iNKT TCR–CD1d–antigen binding under the assumption that different parts of the iNKT TCR (i.e., different CDR loops) are involved in recognizing either agonistic (α-GalCer) or nonagonistic (PC) CD1d–antigens. We hypothesize that agonistic binding of iNKT TCRs to CD1d–antigen molecules requires two conditions, namely recognition of the CD1d–antigen complex by CDR3α as well as stable docking of the CDR2β loop onto the α2 helix of CD1d, involving a charge interaction between Glu57 (iNKT TCR) with Arg79 (CD1d). Neither condition would be fulfilled in the case of PC-loaded CD1d proteins.

In conclusion, this study demonstrates that human CD1d–α-GalCer–specific TCRs are structurally indistinguishable from pMHC-specific TCRs and supports the hypothesis that they bind the CD1d molecule in a similar diagonal orientation to that of pMHC-recognizing TCRs. Our data provide compelling evidence that the CDR3 loop of the invariant Vα chain is essential for recognition of the carbohydrate head group of the CD1d ligand, and suggest that the CDR2 loop of the Vβ11 chain is strongly involved in binding to the CD1d protein.

MATERIALS AND METHODS

Generation of Vα24$^+$ and Vα24$^-$, CD1d–α-GalCer–specific T cell clones. Invariant Vα24$^+$/Vβ11$^+$NKT cells were expanded in vitro by stimulation of human peripheral blood mononuclear cells with 100 nM α-GalCer. After 14 d, single CD4$^-$/CD8$^-$ (DN) iNKT cells were sorted into round bottom 96-well plates using a FACSVantage cell sorter and restimulated with irradiated allogenic feeder cells and 100 nM α-GalCer. The Vα24-negative, CD1d–α-GalCer–specific T cell line 5.Y was derived from a buffy coat stimulated with 100 nM α-GalCer in the presence of irradiated allogenic human PBMC. FACSVantage-assisted cloning of Vα24$^-$/CD1d–α-GalCer tetramer$^+$ T cells was carried out as described above for the iNKT cell cloning. All T cell clones were maintained in Iscove's modified Dulbecco's minimum essential medium (Sigma-Aldrich) supplemented with 5% heat-inactivated human serum, 1% streptomycin/penicillamine, and 1% glutamine.

Flow cytometry. 4 wk after restimulation, T lymphocyte clones (1×10^5 cells per staining) were analyzed for purity and viability by FACS using propidium iodide (Sigma-Aldrich), FITC–anti-Vα24 and RPE–anti-Vβ11 (Serotec), as well as Streptavidin-APC–conjugated CD1d–α-GalCer tetramers (41) in combination with FITC–anti-CD3, PerCP–anti-CD4, and RPE–anti-CD8β antibodies (all from BD Pharmingen). All 14 isolated Vα24$^-$, CD1d–α-GalCer tetramer$^+$ T cell clones were also analyzed by CD1d–α-GalCer monomer staining as described (8). In brief, cells were incubated with biotinylated CD1d–α-GalCer monomers on ice for 30 min, washed twice with ice-cold PBS, stained with R-PE-Extraavidin (Sigma-Aldrich) on ice for 30 minutes, and washed again twice with ice-cold PBS. All samples were analyzed on a FACSCalibur flow cytometer, and data were processed using CellQuest software (BD Biosciences).

Preparation of soluble biotinylated CD1d–α-GalCer complexes and CD1d–α-GalCer tetramers. Human biotinlyated CD1d–α-GalCer complexes and Streptavidin-linked CD1d–α-GalCer tetramers were prepared by in vitro refolding from bacterially expressed inclusion bodies and synthetic α-GalCer as previously described (41).

Manufacture of soluble heterodimeric TCRs. The generation of soluble TCR heterodimers was based on the procedure described by Boulter et al. (42). The extracellular region of each TCR chain was individually cloned in the bacterial expression vector pGMT7 and expressed in *E. coli* BL21-DE3 (pLysS). Residues Thr48 and Ser57, respectively, of the α- and β-chain TCR constant region domains were both mutated to cysteine. Expression, refolding, and purification of the resultant dsTCR heterodimers was carried out as described previously (43).

Surface plasmon resonance. Approximately 5,000 response units of streptavidin were linked to a BIAcore CM-5 chip (BIAcore AB) using the amino-coupling kit according to manufacturer's instructions, and CD1d–α-GalCer complexes or control proteins (CD1b–β-galactosylceramide complex, CD1d–ganglioside GM1, and HLA-A2*01-NY-Eso-1(157-165) complex) were flowed over individual flow cells at a concentration of ~50 μg/ml until the response measured ~1,000 response units. Serial dilutions of 5E, 5B, and iNKT dsTCRs (and for some control experiments a HLA-A2*01-NY-Eso-1–specific dsTCR) were then flowed over the relevant flow cells at a rate of 5 μl/min (for equilibrium binding measurements) or 50 μl/min (for kinetic measurements). Responses were recorded in real time on a Biacore 3000 machine at 25°C, and data were analyzed using BIAevaluation software (BIAcore). Equilibrium dissociation constants (K_D values) were determined assuming a 1:1 interaction ($A + B \leftrightarrow AB$) by plotting specific equilibrium binding responses against protein concentrations followed by nonlinear least squares fitting of the Langmuir binding equation, $AB = B \times AB_{max}/(K_D + B)$, and were confirmed by linear Scatchard plot analysis using Origin 6.0 software (Microcal). Kinetic binding parameters (k_{on} and k_{off}) were determined using BIAevaluation software.

Crystallization of TCRs 5E, 5B, and iNKT. 5E, 5B, and iNKT dsTCRs were concentrated to 10 mg/ml in buffer (100 mM NaCl, 10 mM Tris, pH 8.0) and crystallized by the sitting drop vapor diffusion method. The crystallizations of 5E and 5B dsTCRs were set up as nanoliter scale drops (100 nL of protein plus 100 nL of reservoir solution) using a Cartesian Technologies Microsys MIC4000 (Genomic Technologies) (44). Crystallizations of the iNKT dsTCR were set up using 2 μL plus 2 μL drops hand pipetted into microbridges.

Crystals of 5E dsTCR grew at room temperature in 200 mM magnesium sulphate and 20% polyethylene glycol 3350. 5B dsTCR crystals grew at room temperature at a final concentration of 10 mg ml^{-1} in 200 mM di-ammonium tartrate, 20% polyethylene glycol 3350. iNKT dsTCR crystals grew at room temperature at a final concentration of 10 mg ml^{-1} in 0.5 M NaCl, 11% polyethylene glycol 8000, 50 mM HEPES, pH 7.0. Crystals were soaked briefly in per-fluoropolyether oil (PFPE) before being flash cooled and maintained at 100 K in a cryostream.

Diffraction data for the 5E dsTCR were recorded at station ID14-EH2 of the European Synchrotron Radiation Facility (ESRF) with an ADSC Q4 CCD detector. Because of detector overloads at low crystal to detector distance both a high-resolution (175 mm detector distance) and a low-resolution (300 mm detector distance) dataset were collected from the same crystal. The crystal belonged to the spacegroup $P3_221$ (a = b = 64.5 Å, c = 184.9 Å) and both datasets were autoindexed with DENZO and scaled together using SCALEPACK (http://www.hkl-xray.com) (Table I). There was a single molecule in the asymmetric unit and 44% solvent.

Data for the 5B dsTCR were recorded at station 14.2 of the Synchrotron Radiation Source at the Daresbury Laboratory (SRS) with an ADSC Q4 CCD detector. The crystal belonged to the spacegroup $P3_121$ (a = b = 64.0 Å, c = 185.0 Å), with a single molecule in the asymmetric unit and 43% solvent. The diffraction from this crystal gave smeared spots, which required use of a large spot size in DENZO to ensure that the full spot intensities were integrated, and these were then scaled using SCALEPACK (Table I).

That the 5E and 5B dsTCR crystals have almost identical unit cell parameters, yet molecular replacement solutions indicated that they had different space groups related by opposite handed screw axes was surprising. However, all attempts at reindexing to allow the two data sets to be scaled together gave very high χ^2 and R_{merge} values, clearly indicating that they belonged to different space groups.

Data were collected for the iNKT TCR at station ID14-EH1 of the ESRF using an ADSC Q4R CCD detector. The crystal belonged to the spacegroup C2 (a = 289.4 Å, b = 85.0 Å, c = 78.9 Å, β = 103.9 °), with three molecules in the asymmetric unit and 60% solvent. Due to variance in the x-ray beam intensity data, processing statistics were poorer than expected when the data were indexed and integrated with DENZO and SCALEPACK (Table I).

Structure determination and refinement. Both the Crystallography and NMR system (CNS) (45) (http://cns.csb.yale.edu/) and REFMAC CCP4 (46) (http://www.ccp4.ac.uk) suite of programs were used for refinement. Approximately 5% of reflections were set aside for the R_{free} calculations. See Table I for refinement statistics.

The structure of the 5E dsTCR was determined by molecular replacement using the JM22 TCR structure (40) (PDB-entry 1OGA) as the search model in the molecular replacement module of CNS (45). A single strong rotation function peak was found and used in a translation search, two symmetry-related peaks in the space group $P3_221$ were found with a high correlation coefficient and good packing scores. The top scoring solution from this stage was used in subsequent refinement. After initial rigid-body refinement of the Vα, Vβ, Cα, and Cβ domains using CNS, the sequence of JM22 was replaced by the dsTCR 5E sequence, the model rebuilt into F_o-F_c and $2F_o$-F_c electron density and initially refined by simulated annealing using CNS. As the quality of the model improved, refinement used positional refinement, individual B-factor refinement with bulk solvent scaling and overall anisotropic B-factor scaling interspersed with manual rebuilding using COOT (http://www.ysbl.york.ac.uk/~emsley/coot/) (47) and O (http://www.bioxray.dk/~mok/o-files.html). In the final stages, water molecules were added using ARP-wARP (48) on the basis of peaks of at least 3σ in the F_o-F_c electron density maps. The CDR3 loops had weak electron density in the $2F_o$-F_c maps and were rebuilt from simulated annealing omit maps calculated using CNS with the CDR loops omitted from the map calculation. This gave clear density for the path of both the CDR3 α and β loops. To complete refinement, the model was subjected to translation libration screw (TLS) and restrained refinement using REFMAC (49, 50) with the Vα, Vβ, Cα, and Cβ domains defining the TLS groups. The final refined structure had good stereochemistry, as assessed by the program PROCHECK (49; Table I), an R_{work} of 18.8% (R_{free} 26.8%) and comprised residues 3–193 of the α chain, 2–245 of the β chain, and 286 water molecules.

The structure of the 5B dsTCR was determined by molecular replacement using the 5E dsTCR structure as the search model in CNS (45). A single strong rotation function peak was used in a translation search. One unique peak was found in space group $P3_121$ with a high correlation coefficient and good packing. After initial rigid-body refinement of the model Vα, Vβ, Cα, and Cβ domains using CNS, the sequence of 5E TCR was replaced with that of 5B TCR guided by F_o-F_c and $2F_o$-F_c electron density maps calculated with CNS. This modeling was followed by refinement as described for 5E dsTCR. The final refined structure had good stereochemistry, as assessed by the program PROCHECK (49; Table I), an R_{work} of 21.7% (R_{free} 31.8%) and comprised residues 10–193 of the α chain, 3–246 of the β chain, and 61 water molecules. The high R_{free} value and large difference from the R_{work} seen for this structure is not uncommon for TCR structures (unpublished data) and may in part be a consequence of the low completeness of the data, only 87% in the highest resolution shell (2.67–2.60 A), used for refinement.

The structure of the iNKT dsTCR was solved by molecular replacement using the structure of 1MI5 as the input model for the CaspR web interface (http://igs-server.cnrs-mrs.fr/Caspr/index.cgi/). This gave three clearly defined solutions for the three molecules in the asymmetric unit. noncrystallographic symmetry (NCS) restraints were set up for the three molecules within the asymmetric unit, but to improve the statistic data SHP (Structure Homology Program) (51) was then used to superimpose the domains from the final refined 5E dsTCR onto the three iNKT dsTCR molecules in the asymmetric unit. CNS was then used to carry out rigid body refinement on the twelve domains (Vα, Cα, Vβ, and Cβ for each of the three NCS-related molecules), with low restraints placed on the CDR loops. Omitting the CDR loops of the molecule, $2F_o$-F_c and F_o-F_c electron density maps were calculated with CNS, and the sequence of the 5E dsTCR was replaced with sequence of the dsTCR iNKT in O. Simulated annealing refinement was cycled with manual rebuilding of the molecule guided by $2F_o$-F_c and F_o-F_c electron density maps in O. The CDR loops were built into the resulting electron density from simulated annealing omit maps, initially as polyalanine chains, and as the side-chains became apparent in subsequent cycles of refinement these were replaced with the correct sequence. The stereochemistry of the model was corrected using Calpha (52). Positional and individual B-factor refinement was carried out with CNS using NCS restraints (again with low restraints placed on the CDR loops) in later stages of refinement. The final refined structure had good stereochemistry, as assessed by the program PROCHECK (49; Table I), an R_{work} of 28.3% (R_{free} 35.0%) and for each of the three receptors in the asymmetric unit comprised residues 2–193 of the α chain, 2–245 of the β chain, and no water molecules.

Structural analysis and modeling. Structures of six unique human pMHC class I–restricted αβ TCRs have been reported previously, all of which were solved as complexes with pMHC class I (accession nos.: 1AO7, 1BD2, 2BNQ, 1LP9, 1MI5, and 1OGA) two of which have also been deposited as TCR structures alone (accession nos.: 1KGCis part of 1MI5 and 2BNU is part of 2BNQ). There are currently five unique mouse αβ TCR structures in the PDB, four of them are complexes with pMHC class I (accession nos.: 2CKB, 1FO0, 1KJ2, and 1NAM), three more are TCR

structures alone (1TCR, 1NFD, and 1KB5), of these 1TCR and 1KB5 are also the TCR part in 2CKB and 1KJ2, respectively. TCR N15 has only been solved as complex with hamster Fab (1NFD). Superpositions to obtain the rmsd values between TCR structures were done with the program IMPOSE (unpublished program; Esnouf, R., personal communication). A "core set" of framework residues were chosen: residues 4–24, 35–47, 71–93, and 104–111 of the α chain and residues 5–25, 35–47, 72–96, and 106–114 of the β chain (residue numbering as in iNKT-TCR) for superpositions of the dsTCRs as well as of the human TCRs. This selection was slightly changed in the β chain for superpositions of the mouse TCRs, here residues 72–83 and 88–96 (86–96 in those cases residues 88 and 89 were missing) were selected instead of residues 72–96.

Previous efforts to generate models for TCR–CD1 glycolipid complexes (by substituting CD1-glycolipid structures into the position of pMHC in TCR–pMHC complexes) resulted in significant steric clashes between the CD1 molecule and the TCR (53). However, within the observed range of diagonal orientations seen for the TCR interaction footprint on the pMHC peptide binding groove, these clashes were minimized for complexes with TCR orientations at the closer to parallel, rather than orthogonal, extremes of the range (unpublished data; Batuwangala, T., personal communication). This TCR orientation is exemplified by that of the murine TCR 2C in the crystal structure of 2C-dEV8-H-2K^b (accession no. 2CKB; reference 34), and after updating our assessment of possible docking orientations in the light of recent additions to the data base of TCR–pMHC complex structures, we selected this complex as the basis for a modeling exercise (as described in Materials and methods). To generate docking models for the binding of the iNKT, 5E and 5B dsTCRs, onto human CD1d–α-GalCer, we first superimposed each of the three dsTCRs onto the position of the TCR 2C in the crystal structure of the 2C-dEV8-H-2K^b complex; the pairwise superpositions were based on the Vα chains and used program SHP (51). Subsequently, human CD1d–α-GalCer (accession no. 1ZT4;reference 16) was superimposed onto the position of dEV8-H-2K^b in the TCR–pMHC complex based on superposition of the α1/α2 domains. No attempt was made to optimize the interaction surfaces generated by these rigid body superpositions.

Structural figures were prepared with Bobscript (47), Raster3D (48), and Grasp_(http://trantor.bioc.columbia.edu/grasp/).

Accession numbers. Coordinates and structure factors have been deposited in the Protein Data Bank under accession nos. 2CDE(iNKT-TCR), 2CDF(TCR 5E), and 2CDG(TCR 5B).

Online supplemental materials. FACS staining data for the two TCRs 5E and 5B is presented in Fig. S1. Composite OMIT electron density maps for the α chains (Fig. S2) and for the β chains (Fig. S3) of the structures of all three TCRs are shown. The conformations of Arg79, Ser76, and Asp80 in three published human and mouse CD1d structures are illustrated in Fig. S4, and the potential surfaces of the three TCRs calculated using GRASP are depicted in Fig. S5. Figs. S1–S5 are available at http://www.jem.org/cgi/content/full/jem.20052369/DC1.

The authors wish to thank all STRUBI members for assistance and helpful discussions, explicitly John Grimes, Robert Esnouf, and Rebecca Hamer. We are also grateful to the staff of the ESRF and The European Molecular Biology Laboratory in Grenoble and at the SRS in Daresbury, Warrington, for assistance with x-ray data collection. We acknowledge use of crystallization facilities provided by the Medical Research Council–funded Oxford Protein Production Facility and The European Commission Integrated Programme (SPINE; grant code QLRT-2001-00988).

S.D. Gadola is a Max Cloëtta Foundation Principal Research Fellow, and E.Y. Jones is a Cancer Research UK Principal Research Fellow. This work was funded by the Swiss National Science Foundation (3200-068070 and 3200-069338 to S.D. Gadola), Cancer Research UK (C399-A2291 to V. Cerundolo and C375-A2320 to E.Y. Jones), the Swiss Multiple Sclerosis Foundation, Kamillo Eisner Foundation, and Kurt und Senta Herrmann Stiftung (to S.D. Gadola), US Cancer Research Institute, and the UK Medical Research Council. J. Marles-Wright is a recipient of a Cancer Research UK studentship.

The authors have no other conflicting financial interests.

Submitted: 28 November 2005
Accepted: 2 February 2006

REFERENCES

1. Brigl, M., and M.B. Brenner. 2004. CD1: antigen presentation and T cell function. *Annu. Rev. Immunol.* 22:817–890.
2. Porcelli, S.A., and R.L. Modlin. 1999. The CD1 system: antigen-presenting molecules for T cell recognition of lipids and glycolipids. *Annu. Rev. Immunol.* 17:297–329.
3. Porcelli, S., C.E. Yockey, M.B. Brenner, and S.P. Balk. 1993. Analysis of T cell antigen receptor (TCR) expression by human peripheral blood CD4−8− α/β T cells demonstrates preferential use of several V β genes and an invariant TCR α chain. *J. Exp. Med.* 178:1–16.
4. Lantz, O., and A. Bendelac. 1994. An invariant T cell receptor α chain is used by a unique subset of major histocompatibility complex class I–specific CD4+ and CD4−8− T cells in mice and humans. *J. Exp. Med.* 180:1097–1106.
5. Behar, S.M., and S. Cardell. 2000. Diverse CD1d-restricted T cells: diverse phenotypes, and diverse functions. *Semin. Immunol.* 12:551–560.
6. Van Rhijn, I., D.C. Young, J.S. Im, S.B. Levery, P.A. Illarionov, G.S. Besra, S.A. Porcelli, J. Gumperz, T.Y. Cheng, and D.B. Moody. 2004. CD1d-restricted T cell activation by nonlipidic small molecules. *Proc. Natl. Acad. Sci. USA.* 101:13578–13583.
7. Kawano, T., J. Cui, Y. Koezuka, I. Toura, Y. Kaneko, K. Motoki, H. Ueno, R. Nakagawa, H. Sato, E. Kondo, et al. 1997. CD1d-restricted and TCR-mediated activation of vα14 NKT cells by glycosylceramides. *Science.* 278:1626–1629.
8. Gadola, S.D., N. Dulphy, M. Salio, and V. Cerundolo. 2002. Vα24-JαQ-independent, CD1d-restricted recognition of α-galactosylceramide by human CD4(+) and CD8αβ(+) T lymphocytes. *J. Immunol.* 168:5514–5520.
9. Chang, D.H., K. Osman, J. Connolly, A. Kukreja, J. Krasovsky, M. Pack, A. Hutchinson, M. Geller, N. Liu, R. Annable, et al. 2005. Sustained expansion of NKT cells and antigen-specific T cells after injection of α-galactosyl-ceramide loaded mature dendritic cells in cancer patients. *J. Exp. Med.* 201:1503–1517.
10. Gapin, L., J.L. Matsuda, C.D. Surh, and M. Kronenberg. 2001. NKT cells derive from double-positive thymocytes that are positively selected by CD1d. *Nat. Immunol.* 2:971–978.
11. Benlagha, K., D.G. Wei, J. Veiga, L. Teyton, and A. Bendelac. 2005. Characterization of the early stages of thymic NKT cell development. *J. Exp. Med.* 202:485–492.
12. Chen, J.L., G. Stewart-Jones, G. Bossi, N.M. Lissin, L. Wooldridge, E.M. Choi, G. Held, P.R. Dunbar, R.M. Esnouf, M. Sami, et al. 2005. Structural and kinetic basis for heightened immunogenicity of T cell vaccines. *J. Exp. Med.* 201:1243–1255.
13. Garcia, K.C., L. Teyton, and I.A. Wilson. 1999. Structural basis of T cell recognition. *Annu. Rev. Immunol.* 17:369–397.
14. Al-Lazikani, B., A.M. Lesk, and C. Chothia. 2000. Canonical structures for the hypervariable regions of T cell αβ receptors. *J. Mol. Biol.* 295:979–995.
15. Rudolph, M.G., and I.A. Wilson. 2002. The specificity of TCR/pMHC interaction. *Curr. Opin. Immunol.* 14:52–65.
16. Koch, M., V.S. Stronge, D. Shepherd, S.D. Gadola, B. Mathew, G. Ritter, A.R. Fersht, G.S. Besra, R.R. Schmidt, E.Y. Jones, and V. Cerundolo. 2005. The crystal structure of human CD1d with and without α-galactosylceramide. *Nat. Immunol.* 6:819–826.
17. Bradbury, A., K.T. Belt, T.M. Neri, C. Milstein, and F. Calabi. 1988. Mouse CD1 is distinct from and co-exists with TL in the same thymus. *EMBO J.* 7:3081–3086.
18. Balk, S.P., P.A. Bleicher, and C. Terhorst. 1991. Isolation and expression of cDNA encoding the murine homologues of CD 1. *J. Immunol.* 146:768–774.
19. Zeng, Z., A.R. Castano, B.W. Segelke, E.A. Stura, P.A. Peterson, and I.A. Wilson. 1997. Crystal structure of mouse CD1: An MHC-like fold with a large hydrophobic binding groove. *Science.* 277:339–345.
20. Zajonc, D.M., C. Cantu III, J. Mattner, D. Zhou, P.B. Savage, A. Bendelac, I.A. Wilson, and L. Teyton. 2005. Structure and function of

a potent agonist for the semi-invariant natural killer T cell receptor. *Nat. Immunol.* 6:810–818.
21. Giabbai, B., S. Sidobre, M.D. Crispin, Y. Sanchez-Ruiz, A. Bachi, M. Kronenberg, I.A. Wilson, and M. Degano. 2005. Crystal structure of mouse CD1d bound to the self ligand phosphatidylcholine: a molecular basis for NKT cell activation. *J. Immunol.* 175:977–984.
22. Grant, E.P., M. Degano, J.P. Rosat, S. Stenger, R.L. Modlin, I.A. Wilson, S.A. Porcelli, and M.B. Brenner. 1999. Molecular recognition of lipid antigens by T cell receptors. *J. Exp. Med.* 189:195–205.
23. Grant, E.P., E.M. Beckman, S.M. Behar, M. Degano, D. Frederique, G.S. Besra, I.A. Wilson, S.A. Porcelli, S.T. Furlong, and M.B. Brenner. 2002. Fine specificity of TCR complementarity-determining region residues and lipid antigen hydrophilic moieties in the recognition of a CD1-lipid complex. *J. Immunol.* 168:3933–3940.
24. Burdin, N., L. Brossay, M. Degano, H. Iijima, M. Gui, I.A. Wilson, and M. Kronenberg. 2000. Structural requirements for antigen presentation by mouse CD 1. *Proc. Natl. Acad. Sci. USA.* 97:10156–10161.
25. Zajonc, D.M., M.D. Crispin, T.A. Bowden, D.C. Young, T.Y. Cheng, J. Hu, C.E. Costello, P.M. Rudd, R.A. Dwek, M.J. Miller, et al. 2005. Molecular mechanism of lipopeptide presentation by CD1a. *Immunity.* 22:209–219.
26. Havran, W.L., and J.P. Allison. 1988. Developmentally ordered appearance of thymocytes expressing different T-cell antigen receptors. *Nature.* 335:443–445.
27. Matsuda, J.L., L. Gapin, N. Fazilleau, K. Warren, O.V. Naidenko, and M. Kronenberg. 2001. Natural killer T cells reactive to a single glycolipid exhibit a highly diverse T cell receptor β repertoire and small clone size. *Proc. Natl. Acad. Sci. USA.* 98:12636–12641.
28. van der Merwe, P.A., and S.J. Davis. 2003. Molecular interactions mediating T cell antigen recognition. *Annu. Rev. Immunol.* 21:659–684.
29. Sidobre, S., O.V. Naidenko, B.C. Sim, N.R. Gascoigne, K.C. Garcia, and M. Kronenberg. 2002. The Vα14 NKT cell TCR exhibits high-affinity binding to a glycolipid/CD1d complex. *J. Immunol.* 169:1340–1348.
30. Sidobre, S., K.J. Hammond, L. Benazet-Sidobre, S.D. Maltsev, S.K. Richardson, R.M. Ndonye, A.R. Howell, T. Sakai, G.S. Besra, S.A. Porcelli, and M. Kronenberg. 2004. The T cell antigen receptor expressed by Vα14i NKT cells has a unique mode of glycosphingolipid antigen recognition. *Proc. Natl. Acad. Sci. USA.* 101:12254–12259.
31. Cantu, C., III, K. Benlagha, P.B. Savage, A. Bendelac, and L. Teyton. 2003. The paradox of immune molecular recognition of α-galactosylceramide: low affinity, low specificity for CD1d, high affinity for αβTCRs. *J. Immunol.* 170:4673–4682.
32. Jorgensen, J.L., U. Esser, B. Fazekas de St Groth, P.A. Reay, and M.M. Davis. 1992. Mapping T-cell receptor-peptide contacts by variant peptide immunization of single-chain transgenics. *Nature.* 355:224–230.
33. Garboczi, D.N., P. Ghosh, U. Utz, Q.R. Fan, W.E. Biddison, and D.C. Wiley. 1996. Structure of the complex between human T-cell receptor, viral peptide and HLA-A 2. *Nature.* 384:134–141.
34. Garcia, K.C., M. Degano, L.R. Pease, M. Huang, P.A. Peterson, L. Teyton, and I.A. Wilson. 1998. Structural basis of plasticity in T cell receptor recognition of a self peptide-MHC antigen. *Science.* 279:1166–1172.
35. Fischer, K., E. Scotet, M. Niemeyer, H. Koebernick, J. Zerrahn, S. Maillet, R. Hurwitz, M. Kursar, M. Bonneville, S.H. Kaufmann, and U.E. Schaible. 2004. Mycobacterial phosphatidylinositol mannoside is a natural antigen for CD1d-restricted T cells. *Proc. Natl. Acad. Sci. USA.* 101:10685–10690.
36. Zhou, D., J. Mattner, C. Cantu III, N. Schrantz, N. Yin, Y. Gao, Y. Sagiv, K. Hudspeth, Y.P. Wu, T. Yamashita, et al. 2004. Lysosomal glycosphingolipid recognition by NKT cells. *Science.* 306:1786–1789.
37. Bendelac, A., M.N. Rivera, S.H. Park, and J.H. Roark. 1997. Mouse CD1-specific NK1 T cells: development, specificity, and function. *Annu. Rev. Immunol.* 15:535–562.
38. Schumann, J., R.B. Voyle, B.Y. Wei, and H.R. MacDonald. 2003. Cutting edge: influence of the TCR Vβ domain on the avidity of CD1d:α-galactosylceramide binding by invariant Vα14 NKT cells. *J. Immunol.* 170:5815–5819.
39. Stanic, A.K., R. Shashidharamurthy, J.S. Bezbradica, N. Matsuki, Y. Yoshimura, S. Miyake, E.Y. Choi, T.D. Schell, L. Van Kaer, S.S. Tevethia, et al. 2003. Another view of T cell antigen recognition: cooperative engagement of glycolipid antigens by Vα14Jα18 natural T(iNKT) cell receptor. *J. Immunol.* 171:4539–4551.
40. Stewart-Jones, G.B., A.J. McMichael, J.I. Bell, D.I. Stuart, and E.Y. Jones. 2003. A structural basis for immunodominant human T cell receptor recognition. *Nat. Immunol.* 4:657–663.
41. Karadimitris, A., S. Gadola, M. Altamirano, D. Brown, A. Woolfson, P. Klenerman, J.L. Chen, Y. Koezuka, I.A. Roberts, D.A. Price, et al. 2001. Human CD1d-glycolipid tetramers generated by *in vitro* oxidative refolding chromatography. *Proc. Natl. Acad. Sci. USA.* 98: 3294–3298.
42. Boulter, J.M., M. Glick, P.T. Todorov, E. Baston, M. Sami, P. Rizkallah, and B.K. Jakobsen. 2003. Stable, soluble T-cell receptor molecules for crystallization and therapeutics. *Protein Eng.* 16:707–711.
43. Willcox, B.E., G.F. Gao, J.R. Wyer, C.A. O'Callaghan, J.M. Boulter, E.Y. Jones, P.A. van der Merwe, J.I. Bell, and B.K. Jakobsen. 1999. Production of soluble αβT-cell receptor heterodimers suitable for biophysical analysis of ligand binding. *Protein Sci.* 8:2418–2423.
44. Mieza, M.A., T. Itoh, J.Q. Cui, Y. Makino, T. Kawano, K. Tsuchida, T. Koike, T. Shirai, H. Yagita, A. Matsuzawa, et al. 1996. Selective reduction of Vα14+ NK T cells associated with disease development in autoimmune-prone mice. *J. Immunol.* 156:4035–4040.
45. Brunger, A.T., P.D. Adams, G.M. Clore, W.L. DeLano, P. Gros, R.W. Grosse-Kunstleve, J.S. Jiang, J. Kuszewski, M. Nilges, N.S. Pannu, et al. 1998. Crystallography & NMR system: A new software suite for macromolecular structure determination. *Acta Crystallogr. D Biol. Crystallogr.* 54(Pt 5):905–921.
46. Collaborative Computational Project, Number 4. 1994. The CCP4 suite: programs for protein crystallography. *Acta Crystallogr. D Biol. Crystallogr.* 50:760–763.
47. Emsley, P., and K. Cowtan. 2004. Coot: model-building tools for molecular graphics. *Acta Crystallogr. D Biol. Crystallogr.* 60:2126–2132.
48. Morris, R.J., A. Perrakis, and V.S. Lamzin. 2003. ARP/wARP and automatic interpretation of protein electron density maps. *Methods Enzymol.* 374:229–244.
49. Murshudov, G.N., A.A. Vagin, and E.J. Dodson. 1997. Refinement of macromolecular structures by the maximum-likelihood method. *Acta Crystallogr. D Biol. Crystallogr.* 53:240–255.
50. Winn, M.D., M.N. Isupov, and G.N. Murshudov. 2001. Use of TLS parameters to model anisotropic displacements in macromolecular refinement. *Acta Crystallogr. D Biol. Crystallogr.* 57:122–133.
51. Stuart, D.I., M. Levine, H. Muirhead, and D.K. Stammers. 1979. Crystal structure of cat muscle pyruvate kinase at a resolution of 2.6 A. *J. Mol. Biol.* 134:109–142.
52. Esnouf, R.M. 1997. Polyalanine reconstruction from Calpha positions using the program CALPHA can aid initial phasing of data by molecular replacement procedures. *Acta Crystallogr. D. Biol. Crystallogr.* 53(Pt6):665–672.
53. Batuwangala, T., D. Shepherd, S.D. Gadola, K.J. Gibson, N.R. Zaccai, A.R. Fersht, G.S. Besra, V. Cerundolo, and E.Y. Jones. 2004. The crystal structure of human CD1b with a bound bacterial glycolipid. *J. Immunol.* 172:2382–2388.